JOURNAL OF OPTOELECTRONICS AND ADVANCED MATERIALS, Vol. 12, No. 7, July 2010, p. 1490 - 1497

Influence of annealing temperature on structural and optical properties of mesoporous TiO_2 thin films prepared by sol-gel templating technique

B. YARMAND*, S. K. SADRNEZHAAD[a]
Department of New Materials, Materials and Energy Research Center, Karaj, Iran
[b]*Department of Material Science and Engineering, Sharif University of Technology, Tehran, Iran*

TiO_2 thin films with mesoporous structure were deposited on quartz substrate by sol-gel dip coating. The structural, morphological and optical properties of the films were characterized by X-ray diffraction (XRD), simultaneous thermal analysis (STA), Fourier transform infrared spectroscopy (FT-IR), Brunauer–Emmett–Teller (BET), atomic force microscopy (AFM), transmission electron microscopy (TEM) and UV/Vis transmittance spectroscopy. Crystallization of the anatase phase was initiated at 300°C. Its transformation to the rutile phase occurred at 700°C. Anatase and rutile crystallites initially sized 3.2 and 15.3nm, respectively. The anatase phase was under tension; but the rutile phase was under compression. Increasing the annealing temperature decreased the strains in both phases and the specific surface area of the films; but increased the sizes of the pores. At higher annealing temperatures, the transmittance maxima of the films decreased in the visible region and the absorption edges shifted to longer wavelengths. Optical band gap of the films annealed at 300 and 900°C was 3.61 and 3.25eV, respectively. The refractive index of the films increased from 1.71 to 1.92 and their porosity decreased from 63.9 to 49.7% as the annealing temperature increased from 300 to 700°C.

(Received June 15, 2010; accepted July 14, 2010)

Keywords: Mesoporous TiO_2, Thin films, Sol-gel templating technique, structural and optical properties.

1. Introduction

Research interest has multiplied recently on titanium dioxide (TiO_2) phases due to their extraordinary optical and electrical properties as well as easy synthesis and great chemical stability [1-3]. TiO_2 has a wide band gap with attractive semiconductor properties mainly dependent on its different crystalline forms being appeared as anatase, rutile and brookite. Anatase is photocatalytically much more active than rutile [4, 5]. Rutile has good stability and high refractive index. Such features make it most suitable for protective coatings deposited on lenses [6].

As a result of their low cost and versatility, mesoporous TiO_2 thin films (MTTF) are attractive new materials for photocatalysis [7, 8], dye-sensitized solar cells [9, 10], sensors [11], rechargeable lithium batteries [12, 13] and many other applications.

Various deposition techniques such as electron beam evaporation [14], chemical vapor deposition (CVD) [15, 16], pulsed laser deposition [17], reactive sputtering technique [18], ultrasonic irradiation process [19], spray pyrolysis [20], hydrothermal process [21] and sol-gel methods [22] have been used for production of TiO_2 films. These techniques are highly capable of controlling nucleation and growth rates and tailoring the chemical and physical properties of the thin layers.

Besides the above methods, the sol-gel technique can be considered as most influential technique for preparation of the mesoporous thin layers. It can provide good homogeneity, uniform composition and large specific areas via mild processing conditions [23, 24]. A combination of the evaporation-induced self-assembly (EISA) using structure-directing polymer (template) with complexation of molecular inorganic species in precursor can be used to prepare the mesoporous films through sol-gel process. When the template polymer is exposed to extraction by thermal treatment, the organic–inorganic mesophase is transformed into a controlled-porosity mesoporous material [25, 26].

Structural and optical properties of MTTF produced by sol-gel techniques have been found to depend mainly on the experimental conditions during deposition and annealing stages. This work is mainly focused, thus, on the effect of the annealing temperature on structural, morphological and optical properties of the mesoporous TiO_2 thin films produced by sol-gel method. Evaporation induced self-assembly was utilized for provision of low-cost direct mesostructure layer production.

2. Experimental

2.1 Materials and chemicals

Titanium tetraisopropoxide [Ti $(O{\cdot}i\text{-}C_3H_7)_4$] 98% (Merck) was used as precursor; hydrochloric acid (HCl) 32% (Merck) as catalyst, non-ionic triblock copolymer surfactant Pluronic P123 [poly-(ethylene oxide) poly-

(propylene oxide) poly-(ethylene oxide) EO_{20}–PO_{70}–EO_{20}] (Aldrich) as template and ethanol (C_2H_5OH) 99.9% (Merck) as solvent. All as received chemicals were used in the experiments. Quartz slide substrates were applied for deposition of the thin layers.

2.2. Production of mesoporous TiO_2 thin film

Mesoporous TiO_2 thin films were prepared by self-assembly of the P123 triblock copolymer surfactant in sol-gel solution [27]. Room temperature stirring of 5 g Ti (O·i-$C_3H_7)_4$ with 3.2 g HCl for 10 min resulted in hydrolysis to occur. The hydrolyzed sol was mixed with 1 g P123 surfactant being dissolved in 21 g ethanol under stirring for 10 min at room temperature. Quartz substrates were subsequently coated with dipping and withdrawing speed of 60 mm/min. The films were then aged at 10°C for 24 h under controlled humidity of 65-75%. The samples were finally annealed in a tube furnace at different temperatures ranging from 300 to 900°C for 1 h under air with a heating rate of 1.0°C/min. Before coating, the quartz substrate having dimensions of 2.5×1.25×0.2 cm^3 were degreased, thoroughly cleaned and dried in an oven at 120°C for 30 min.

2.3. Characterization

Phase identification, crystallite size and unit cell properties of the films were examined by an X-ray diffractometer with Cu-K_α radiation and Ni filter operated at 40 kV and 30 mA (Philips, PW3710). The scanning range was from 20 to 80° with a scanning rate of 0.25°min^{-1}. Thermal analysis was carried out using PL-STA 1640. Measurements were carried out with a heating rate of 5°C/min at 30 to 1000°C under air. Chemical composition of the films was characterized using Fourier transform infrared spectroscopy (Perkin Elmer, Spectrum 400) in the range of 400-4000 cm^{-1}. The specific surface area of the films was determined through nitrogen adsorption/desorption isotherms (BELSORP 2). The Brunauer–Emmet–Teller (BET) specific surface area was calculated from the linear part of the BET plot (P/P_0 = 0.05 – 0.35). The pore size distribution plots were obtained by using the Barret–Joyner–Halenda (BJH) model. The surface relief and morphology of the films were observed using atomic force microscopy (Auto probe, CP) and transmission electron microscopy (Philips, CM200 FEG), respectively. The optical transmittance spectra of the films were recorded using a UV/Vis spectrophotometer (Perkin Elmer, Lambda 25) with a scanning rate of 60 nm/min in the wavelength range of 200 – 800 nm.

3. Results and discussion

3.1. Structural studies

The wide-angle XRD patterns of powders scraped from the mesoporous TiO_2 thin films annealed at different temperatures are shown in Fig. 1. It is found that the mesoporous TiO_2 thin film prepared at room temperature is amorphous. The anatase peaks appeared at 300°C explaining the nucleation of anatase crystals and beginning of phase transition from amorphous to anatase phase. By increasing temperature from 300 to 700°C, the intensities of the anatase peaks were increased corresponding to the crystallite improvement. It can be observed that rutile peaks with low intensities appear at 700°C. This explains a transition from anatase to rutile phase. By increasing the temperature to 800°C, the intensities of the anatase peaks decrease, while those of the rutile peaks enhance. When the annealing temperature increases further to 900°C, anatase peaks completely disappear and the rutile peaks greatly rises. The strongest peak observed for anatase and rutile phases at different temperatures are (101) 2θ=25.4° and (110) 2θ=27.4°, respectively. No peaks are observed that might confirm the presence of the brookite phase or other compounds like carbon-containing impurity phases.
The average crystallite size of the phases in mesoporous TiO_2 thin films can be calculated from the XRD data by using Scherer's equation [28]:

$$D = \frac{k\lambda}{B\cos\theta}$$

where D is the average crystallite size, λ is the applied X-ray wavelength (λ=1.5406 Å), k=0.90 which is a constant, θ is the diffraction angle in degree and B is the full width at half maximum (FWHM) of the diffraction peak observed in radians. The mass fraction of rutile phase of mesoporous TiO_2 thin films in the absence of brookite phase can be estimated by the following equation [29]:

$$X_{Rutile} = \frac{1}{1 + K\left(I_A / I_R\right)}$$

where I_A and I_R are the intensity of the anatase (101) and rutile (110) reflections, respectively. The empirical constant K is determined via an XRD analysis of samples with known proportions of pure anatase and pure rutile and is equal to 0.79. Fig. 2 shows the effect of annealing temperature on crystallite size of the phases and rutile content of mesoporous TiO_2 thin films. As the annealing temperature increases, the crystallites within the phases continue to grow. The crystallite size of the anatase phase increases about seven times from 3.2 to 22.7 nm as the annealing temperature increases from 300 to 800°C. The crystallite size of the rutile phase at 700°C is 15.3 nm and increases to 27.8 nm at 900°C. The amount of rutile phase increases from 11.1% at 700°C to 100% at 900°C.

Mesoporous TiO_2 thin films have very small crystallite sizes. This results due to using P123 as a template [23].

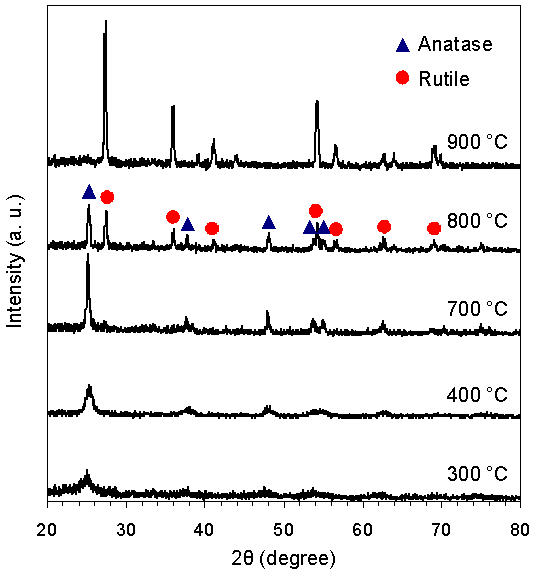

Fig. 1. Wide-angle XRD patterns of mesoporous TiO_2 samples annealed at temperatures given in the figure.

The anatase and rutile phases have a tetragonal unit cell and the lattice parameters can be calculated from two appropriate reflections (hkl) by using the following correlation [28]:

$$\frac{1}{d^2} = \frac{h^2 + k^2}{a^2} + \frac{l^2}{c^2}$$

where d is the measured space of (hkl) planes, which is determined by Bragg's Law, h, k and l are the indexes of crystalline plane relevant to the measured d-spacing respectively and a and c are the lattice parameters of a tetragonal structure. Lattice strain of the phases can be calculated from the full width at half maximum (FWHM) of mean peaks by using Hall's Eq [28]:

$$B\cos\theta = \frac{k\lambda}{D} + 2\varepsilon\sin\theta$$

where ε is the Lattice strain estimated from the slope of the curve Bcosθ vs. 2sinθ. The calculated lattice parameters and lattice strains are shown in Table 1 against the annealing temperature. It can be observed in Table 1 that the lattice constant a of both phases decreases with the annealing temperature; whereas the lattice constant c of the anatase phase increases with the annealing temperature. In the rutile phase, both lattice constants decrease with the annealing temperature. The amounts of lattice constants for anatase phase at 800°C and the rutile phase at 900°C are close to the reported bulk values [30]. It is found that anatase and rutile phases are under tensile and compression strain, respectively. As the annealing temperature increases, the strains in both phases decreases which is attributed to decrease in the lattice imperfections.

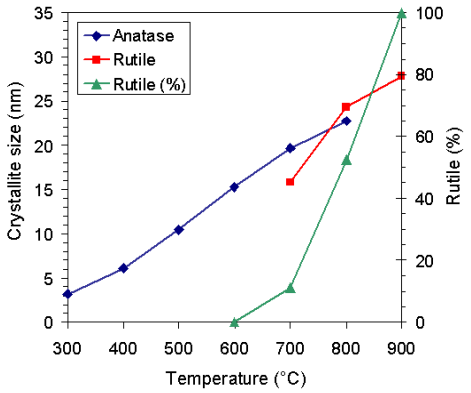

Fig. 2. Variation of crystallite size and rutile content with the annealing temperature.

3.2. Thermal analysis

Thermogravimetry-diffrentioal thermal analysis curves of the powders scraped from mesoporous TiO_2 thin film are shown in Fig. 3. In DTA curve, an exothermic large peak is observed at 250°C. This peak is related to the combustion of the organic compound which results in its removal. There is another exothermic small board peak in the temperature range 300-350°C showing crystallization of the anatase phase. The crystallization temperature of the anatase phase is not clearly observable due to the fact that their temperature overlaps with the decomposition temperature of the organic compound. The next small exothermic peak in the temperature range 720-730°C shows the crystallization of the rutile phase.

Table 1. Lattice parameters and lattice strains of mesoporous TiO_2 thin films versus the annealing temperature.

Annealing temperature	Phase	Lattice parameters (Å)		Lattice strains
		a	c	
300	Anatase	3.7921	9.4541	0.0326
400	Anatase	3.7893	9.4698	0.0146
500	Anatase	3.7874	9.4807	0.0124
600	Anatase	3.7869	9.4937	0.0112
700	Anatase	3.7861	9.5063	0.0109
	Rutile	4.6112	2.9723	-0.0107
800	Anatase	3.7856	9.5152	0.0103
	Rutile	4.6069	2.9691	-0.0087
900	Rutile	4.6043	2.9669	-0.0068

These results are in favor of XRD data obtained. According to the previous researchers, the anatase to rutile phase transition takes place at temperatures around 700°C [31]. It can be inferred that the addition of P123 as a template has no effect on the phase transition

temperatures. According to the TG curve, the weight loss consists of three distinct steps. The first stage is bellow 130°C. Since no further peaks are observable in the DTA curve, it is assumed that the weight loss of 4.1% is due to the loss of physically absorbed water. The second stage weight loss is about 28.5% in temperature range of 180-260°C. This attributes to the removal of the organic compound and the remaining water. In the final stage, a weight loss of 9.4% in the temperature range of 260-400°C contributes to the removal of water during transition of titanium hydroxide to titanium oxide. No changes are found in TG curve at temperatures above 450°C that may imply the complete removal of the organic compound and other materials.

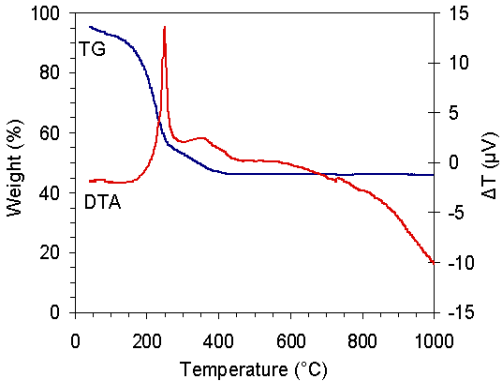

Fig. 3. TG-DTA curves of mesoporous TiO_2 thin film.

3.3. FT-IR studies

The effective removal of the organic compound and degree of hydrolysis reaction were verified by FT-IR, obtained for both the as-prepared and annealed scraped powders of mesoporous TiO_2 thin films. As seen in Fig. 4, the FT-IR spectrum of as-prepared sample shows a peak at 3392 cm^{-1}, which is contributed to the fundamental stretching vibration of hydroxyl groups [32]. The peak at about 1630 cm^{-1} is a result of bending vibration of coordinated H_2O as well as Ti-OH [33]. The next peak at 549 cm^{-1} is due to the stretching vibration of Ti-O bonds in condensed octahedral TiO_6 [32]. Other peaks are attributed to the template. The characteristic absorption peak of (OR) group of titanium isopropoxide, which was the precursor of the sols, is in range 1085–1050 cm^{-1} [34]. Owing to the fact that no absorption peak was detected in this range, it shows that all of the four (OR) groups of titanium isopropoxide were substituted with (OH) groups of water and titanium alkoxide completely transforms to titanium oxide. After annealing at 700 °C, the absorption peaks due to hydroxyl groups, H_2O and P123 are almost removed, as evidenced by the significantly reduced characteristic band.

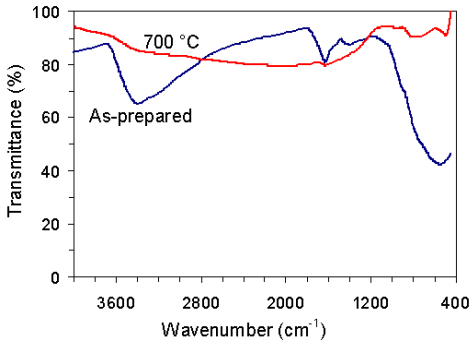

Fig. 4. FT-IR spectra of mesoporous TiO_2 thin films as-prepared and annealed at 700°C.

3.4. Specific surface area

The N_2 adsorption/desorption isotherms and Barrett-Joyner-Halenda (BJH) analysis of adsorption branches of powders scraped from the mesoporous TiO_2 thin films annealed at different temperatures are shown in Fig. 5. All isotherms show a type-4 curve with H1 hysteresis loop that proves the TiO_2 thin films having mesoporous structure [35]. The BJH analysis shows narrow pore size distribution curves indicating mesoporous TiO_2 thin films having uniform pore channels. Variation of the specific surface area and pore size of the mesoporous TiO_2 thin films with the annealing temperature are shown in Table 2. It can be seen that by increasing the annealing temperature, the specific surface area decreases, while the pore diameter increases. These changes in surface and pore properties of the mesoporous TiO_2 thin films with the annealing temperature might be the result of grain growth and remove of small pores.

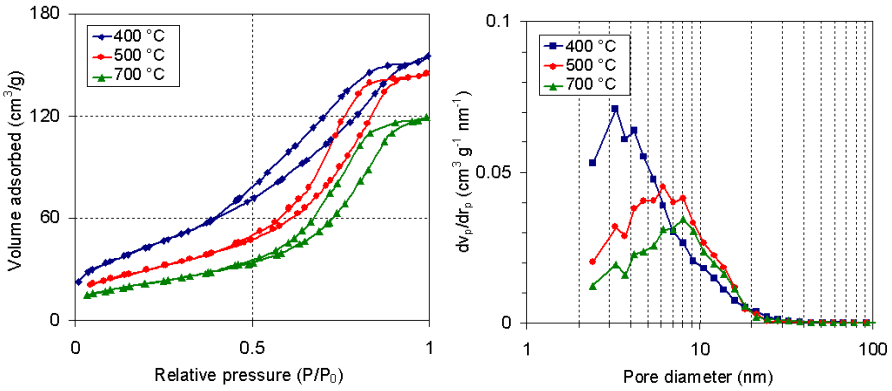

Fig. 5. N_2 adsorption/desorption isotherms and Barret-Joyner-Halenda (BJH) pore size distribution of adsorption branches of mesoporous TiO_2 thin films at different temperatures.

3.5. Morphological characterization

TEM is used to confirm the film mesoporous structure. Fig. 6 shows TEM images of the mesoporous TiO_2 thin film annealed at 400°C. As seen in Fig. 6a, it can be concluded that anatase nanocrystals connect with each other to produce a framework consisting of the mesopores. Fig. 6b shows that anatase nanocrystals have diameters of about 5-7 nm and are randomly oriented. The selected area electron diffractogram exhibits rings with spots confirming the presence of very small anatase nanocrystallites. Fig. 7 shows AFM's 3D topographies of the mesoporous TiO_2 thin films annealled at different temperatures. As is seen, all of the films illustrate uniform hill-valley like morphology. The grain size and surface roughness of the films increase by the annealing temperature. The mean square roughness (rms) of the as-prepared films is 0.488nm. It increases, however, to 3.221nm with increasing to 900°C of the annealing temperature. The increase in roughness is due to increase in the grain size. The thickness of the films is considered being as another crucial factor measured by SEM cross-sectional images. The average thickness of the as-prepared films with one cycle dip coating is estimated to be about 120nm.

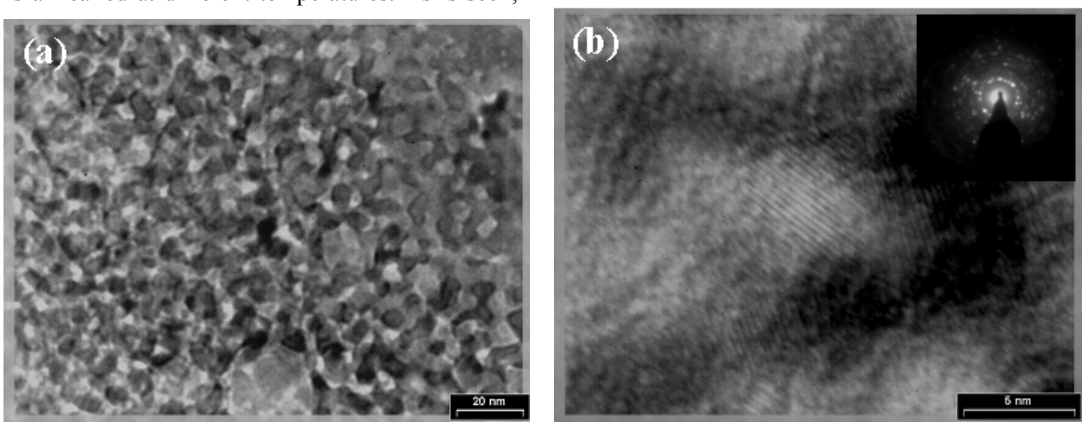

Fig. 6. TEM images of the mesoporous TiO_2 thin film annealed at 400℃ with two magnifications (a) and (b). The inset is a selected area electron diffractogram of the sample.

3.6. Optical characterization

The transmittance spectra of mesoporous TiO_2 thin films annealed at different temperatures are shown in Fig. 8. All films exhibite good transmittance (up to 80%) in the visible region and a sharp fall in the UV region, which corresponds to the band gap. It can be observed that by increasing temperature, transmittance maxima decreases and the absorption edges shift to a longer wavelength. These changes are significantly considerable at 800°C mainly due to the phase transition from anatase to rutile phase as observable in the X-ray diffraction patterns.

Table 2. Specific surface area and pore size of mesoporous TiO_2 thin films annealed at different temperatures.

Annealing temperature	Specific surface area (m^2/g) [by BET]	Mean pore diameter (nm) [by BET]	Average pore diameter (nm) [by BJH, adsorption]	Average pore diameter (nm) [by BJH, desorption]
400	163.43	5.05	3.28	3.28
500	108.91	8.21	6.18	6.18
700	79.23	9.20	8.06	7.38

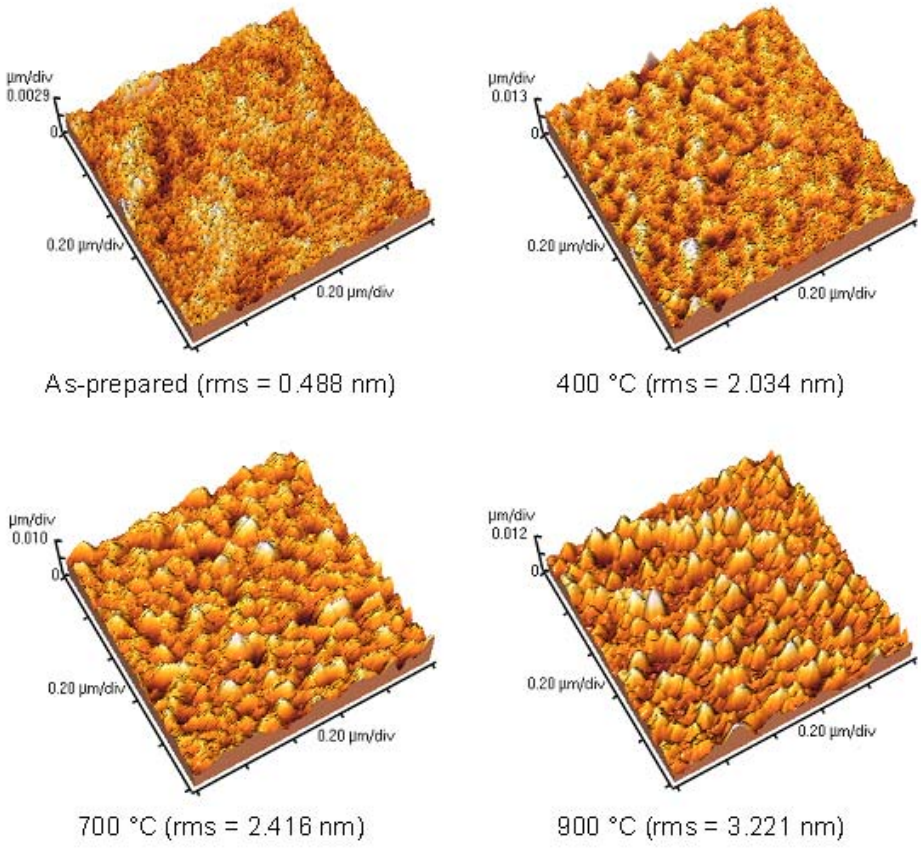

Fig. 7. AFM images of mesoporous TiO_2 thin films as-prepared and annealed at 400℃, 700℃ and 900℃.

The optical band gap (Eg) in a semiconductor is determined by Tauc's equation [36]:

$$\alpha = \frac{k\left(h\upsilon - E_g\right)^n}{h\upsilon}$$

where α is optical absorption coefficient, k is a constant, hν is the photon energy (eV) and n may have different values like 1/2, 2, 3/2 or 3 for allowed direct and indirect and forbidden direct and indirect transitions, respectively [37]. The optical band gap is estimated by extrapolating the straight-line portion of the $(\alpha h\nu)^{1/2}$ vs. hν plot (inset of Fig. 9). The intercept on the energy axis has been noted down for different annealing temperatures. Fig. 9 shows the change in optical band gap with the annealing temperature. The band gap of the film annealed at 300°C is 3.61 eV and it gradually decreases to 3.43 eV after annealing at 700°C. By increasing temperature to 900°C, the band gap significantly decreases to 3.25 eV, which is attributed to anatase to rutile phase transition. The decrease in the optical band gap of the mesoporous TiO_2 thin films with the annealing temperature might be a result of the change in film density and increase in crystallite sizes. The observed values are higher than the band gap of both bulk and thin film TiO_2.

The larger band gap of the film in comparison to their bulk values is contributed to the lattice deformation by an axial strain [38]. The higher band gap observed in our case can be due to the quantum size effects arising from the small size of TiO_2 nano crystallites present in the mesoporous thin film [39].

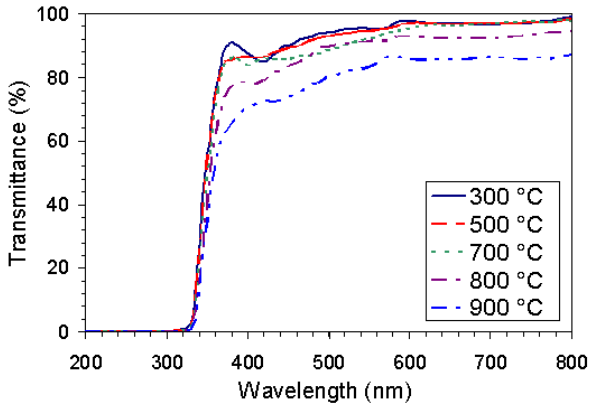

Fig. 8. Optical transmittance spectra of the mesoporous TiO_2 thin films annealed at different temperatures.

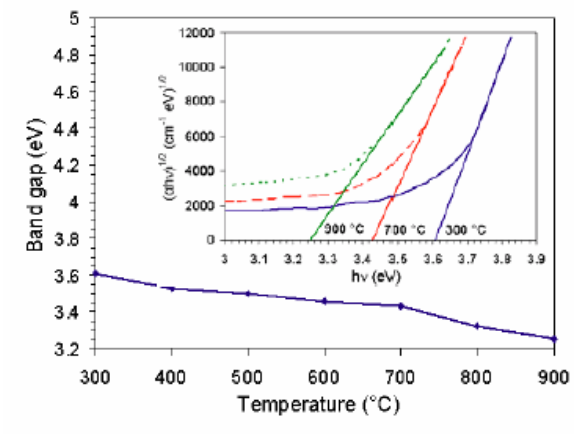

Fig. 9. Optical band gap estimated for mesoporous TiO_2 thin films annealed at different temperatures. The inset is the plot of $(\alpha h\nu)^{1/2}$ vs. $h\nu$.

The refractive index (n) of transparent films is determined using the Swanepoel Envelope method [40]. Maximum transmittance (T_{max}) and minimum transmittance (T_{min}) values are recorded from optical transmittance spectra (Fig. 8). The refractive index can be calculated from the above values by applying the following relation [41]:

$$n = \sqrt{N + \sqrt{N^2 - n_0^2 n_1^2}}$$

Where

$$N = \frac{n_0^2 + n_1^2}{2} + 2n_0 n_1 \frac{T_{max} - T_{min}}{T_{max} T_{min}}$$

where n_0 and n_1 are the refractive indices of air and substrate, respectively, T_{max} is the maximum envelope and T_{min} is the minimum envelope. The refractive index as a function of wavelength is as shown in Fig. 10. It can be seen that the refractive index decreases with increase of wavelength. It is to be noted that the refractive index can further be increased with increasing of the annealing temperature. The values of the refractive index are lower than that of the bulk TiO_2 probably due to the narrow size of the grains [42]. The porosity of the films is calculated using the following equation [43]:

$$Porosity = \left[1 - \left(\frac{n^2 - 1}{n_d^2 - 1}\right)\right] \times 100$$

where n_d is the refractive index of the pore-free TiO_2. It is seen that the porosity of the prepared thin film is quite higher than that of the bulk TiO_2. Fig. 11 shows the variation of the refractive index at 550 nm and the porosity of the mesoporous TiO_2 thin films annealed at different temperatures. The increases in the annealing temperature from 300 to 700°C result in rising of the refractive index from 1.71 to 1.92 and decrease of the porosity from 63.9 to 49.7%. The increase of the refractive index of the film by the annealing temperature can be attributed to the reduction in porosity and film densification.

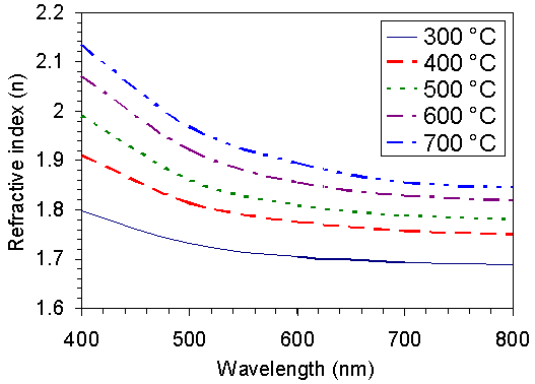

Fig. 10. Variation of the refractive index with wavelength in different temperatures.

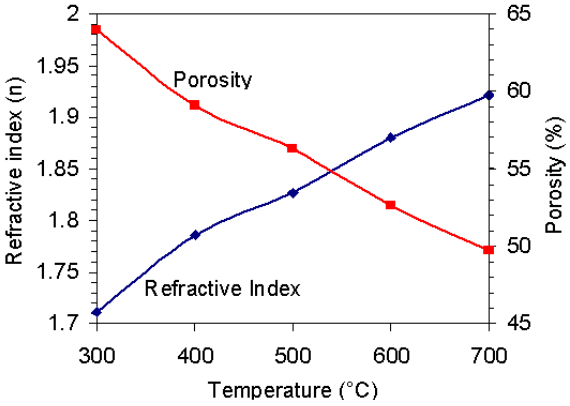

Fig. 11. Variation of the refractive index at 550-nm wavelength and porosity of the mesoporous TiO_2 thin film with the annealing temperature.

4. Conclusions

Mesoporous TiO_2 thin films were successfully prepared on quartz substrate by sol-gel dip coating tempelating technique. The effects of the annealing temperature were examined on structural, morphological and optical properties of the films. XRD-results showed that anatase phase crystallized at 300 °C with crystallite size of 3.2 nm and transformed to rutile phase at 700 °C with crystallite size of 15.3 nm. Anatase and rutile phases were under tensile and compression strain, respectively, and the strain decreased by increasing the annealing temperature. The specific surface area of the thin films annealed at 400 °C was 163.43 m^2/g and decreased to 79.23 m^2/g at 700 °C. The mean square roughness of the as-prepared films was 0.488nm and increased to 3.221 nm with increasing of the annealing temperature to 900 °C. As the temperature increased, the transmittance maxima of the

films decreased in the visible region and the absorption edges shifted to longer wavelengths. The estimated optical band gap of the films decreased from 3.61 to 3.25eV by increasing the annealing temperature from 300 to 900°C. The refractive index of the films increased from 1.71 to 1.92 with enhancement of the temperature from 300 to 700°C and reduction of the porosity from 63.9 to 49.7%.

References

[1] G.K. Mor, O.K. Varghese, M. Paulose, K. Shankar, C.A. Grimes, Sol. Energy Mater. Sol. Cells **90**, 2011 (2006).
[2] R. Zhang, L. Ga, Q. Zhang, Chemosphere **54**, 405 (2004).
[3] D.G. Shchukin, D.V. Sviridov, J. Photochem., C. Photobiol, Photochem. Rev. **7**, 23 (2006).
[4] Y.H. Hsien, C.F. Chang, Y.H. Chen, S. Cheng, Appl. Catal. **B 31**, 241 (2001).
[5] K.M. Schindler, M. Kunst, J. Phys. Chem. **94**, 8222 (1990).
[6] H. Takikawa, T. Matsui, T. Sakakibara, A. Bendavid, P.J. Martin, Thin Solid Films **348**, 145 (1999).
[7] N. Venkatachalam, M. Palanichamy, V. Murugesan, Mater. Chem. Phys. **104**, 454 (2007).
[8] S.Z. Chu, S. Inoue, K. Wada, D. Li, H. Haneda, S. Awatsu, J. Phys. Chem. B **107**, 6586 (2003).
[9] A.C. Arango, L.R. Johnson, V.N. Bliznyuk, Z. Schlesinger, S.A. Carter, Adv. Mater. **12**, 1689 (2000).
[10] A.C. Arango, S.A. Carter, P.J. Brock, Appl. Phys. Lett. **74**, 1698 (1999).
[11] O.K. Varghese, D.W. Gong, M. Paulose, K.G. Ong, E.C. Dickey, C.A. Grimes, Adv. Mater. **15**, 624 (2003).
[12] L. Kavan, J. Rathousky, M. Grätzel, V. Shklover, A. Zukal, J. Phys. Chem. B **104**, 1012 (2000).
[13] O. Wilhelm, S.E. Pratsinis, E. de Chambrier, M. Crouzet, I. Exnar, J. Power Sources **134**, 197 (2004).
[14] D. Bhattacharyya, N.K. Sahoo, S. Thakur, N.C. Das, Thin Solid Films **360**, 96 (2000).
[15] K. Shalini, S. Chandrasekaran, S.A. Shivashanka, J. Cryst. Growth **284**, 388 (2005).
[16] W.Z. Zhang, T. Zhang, W. Yin, G.Y. Cao, Chin. J. Chem. Phys. **20**, 95 (2007).
[17] E. Gyorgy, G. Socol, E. Axente, I.N. Mihailescu, C. Ducu, S. Ciuca, Appl. Surf. Sci. **247**, 429 (2005).
[18] D. Mardare, V. Nica, C.M. Teodorescu, D. Macovei, Surface Science **601**, 4479 (2007).
[19] J.C. Yu, J. Yu, L. Zhang, W. Ho, J. Photochem. Photobiol., A **148**, 263 (2002).
[20] I. Oja, A. Mere, M. Krunks, R. Nisumaa, C.H. Solterbeck, M. Es-Souni, Thin Solid Films **515**, 674 (2006).
[21] S. Kambe, K. Murakoshi, I. Kitamura, Y. Wada, S. Yanagida, H. Kominami, Y. Kera, Sol. Energy Mater. Sol. Cells **61**, 427 (2000).
[22] U. Cernigoj, U. L. Stangar, P. Trebxe, U. O. Kraxovec, S. Gross, Thin Solid Films **495**, 327 (2006).
[23] H. Yun, K. Miyazawa, I. Honma, H. Zhou, M. Kuwabara, Mat. Sci. and Eng. C **23**, 487 (2003).
[24] K. Liu, M. Zhang, K. Shi, H. Fu, Materials Letters **59**, 3308 (2005).
[25] C.J. Brinker, Y.F. Lu, A. Sellinger, H.Y. Fan, Adv. Mater. **11**, 579 (1999).
[26] P. Yang, D. Zhao, D.I. Margolese, B.F. Chmelka, G.D. Stucky, Nature **396**, 152 (1998).
[27] P.C.A. Alberius, K.L. Frindell, R.C. Hayward, E.J. Kramer, Chem. Mater. **14**, 3284 (2002).
[28] B.D. Cullity, Elements of X-ray diffraction, Wesley Publishing Company Inc, London (1978).
[29] R. Spurr, H. Myers, Anal. Chem. **29**, 760 (1957).
[30] H. Tang, F. Levy, H. Berger, P.E. Schmid, Physical Review **52**, 7771 (1995).
[31] N. Negishi, K. Takeuchi, Mater. Lett. **38**, 150 (1999).
[32] M. Crisan, A. Jitianu, M. Zaharescu, F. Mizukami, S. Niwa, J. Dispersion Sci. Technol. **24**, 129 (2003).
[33] B. Klingenberg, M.A. Vannice, Chem. Mater. **8**, 2755 (1996).
[34] G. Socrates, Infrared characteristic group frequencies: Tables and charts, John Wiley & Sons, England (1994).
[35] N. Wark, J. Tschirch, O. Bartels, D. Bahnemann, J. Rathousky, Micropor. Mesopor. Mater. **84**, 247 (2005).
[36] M. Sreemany, S. Sen, Materials Chemistry and Physics **83**, 169 (2004).
[37] D. Bhattacharyya, S. Chaudhuri, A.K. Pal, Vacuum **43**, 313 (1992).
[38] H.C. Ong, A.X.E. Zhu, Appl. Phys. Lett. **80**, 941 (2002).
[39] L. Brus, J. Phys. Chem. **90**, 2555 (1986).
[40] R. Swanepoel, J. Phys. E: Sci. Instrum. **16**, 1214 (1983).
[41] Z. Wang, U. Helmersson, P.O. Kall, Thin Solid Films **405**, 50 (2002).
[42] L. Martinu, D. Poitras, J. Vac. Sci. Technol. A **18**, 2619 (2000).
[43] B.E. Yoldas, P.W. Partlow, Thin Solid Film **129**, 1 (1985).

*Corresponding author: benyamin_yarmand@yahoo.com; byarmand@merc.ac.ir